Research Paper

PAIN

OPEN

A novel intrinsic analgesic mechanism: the enhancement of the conduction failure along polymodal nociceptive C-fibers

Xiuchao Wang[a,b], Shan Wang[c], Wenting Wang[a], Jianhong Duan[a], Ming Zhang[a], Xiaohua Lv[d], Chunxiao Niu[a], Chao Tan[a], Yuanbin Wu[a], Jing Yang[e], Sanjue Hu[a], Junling Xing[a,f,*]

Abstract

Although conduction failure has been observed in nociceptive C-fibers, little is known regarding its significance or therapeutic potential. In a previous study, we demonstrated that C-fiber conduction failure, which is regarded as an intrinsic self-inhibition mechanism, was reduced in circumstances of painful diabetic neuropathy. In this study, we extend this finding in the complete Freund's adjuvant model of inflammatory pain and validate that the degree of conduction failure decreased and led to a greater amount of pain signals conveyed to the central nervous system. In complete Freund's adjuvant–injected animals, conduction failure occurred in a C-fiber-selective, activity-dependent manner and was associated with an increase in the rising slope of the C-fiber after-hyperpolarization potential. To target conduction failure in a therapeutic modality, we used ZD7288, an antagonist of hyperpolarization-activated, cyclic nucleotide–modulated channels which are activated by hyperpolarization and play a pivotal role in both inflammatory and neuropathic pain. ZD7288 promoted conduction failure by suppressing I_h as a mechanism to reduce the rising slope of the after-hyperpolarization potential. Moreover, perineuronal injection of ZD7288 inhibited abnormal mechanical allodynia and thermal hyperalgesia without affecting motor function or heart rate. Our data highlight the analgesic potential of local ZD7288 application and identify conduction failure as a novel target for analgesic therapeutic development.

Keywords: Conduction failure, Nociceptive C-Fiber, HCN, AHP, Pain, Analgesia

1. Introduction

Pharmacological medications for peripheral analgesia, such as local anesthetics and agents targeting the transient receptor potential channel family, are limited by off-target binding and unfavorable side-effect profiles. In clinical trials for these medications, patients have reported numbness, paralysis, and even the loss of autonomic responses. Accordingly, significant efforts have been devoted to the identification of more tolerable and efficacious analgesics as well as methods for the selective blockade of pain signaling.[3,24] This problem is still far from being solved. Although the regulation of nociceptor activity has received significant attention for decades, very limited work has addressed the transduction process that occurs along polymodal nociceptive fibers. Recently, changes in the fidelity of Aα/β-fiber conduction were identified in pathological disease states.[35,38] Furthermore, C-fiber conduction failure was recently observed in painful diabetic neuropathy.[33] These studies provide evidence for the contribution of transduction alterations to abnormal pain; however, the possible impact of this phenomenon on analgesia has been seldom studied, especially in nociceptive C-fibers.

Axonal conduction failure is a state in which nerve impulses are unsuccessfully transmitted along the axon. It is an unusual operation achieved by axon activity that has been observed experimentally in various axons.[8,10] Specific to unmyelinated polymodal C-fibers, the classical idea of conduction suggests that signals originating from the periphery are conveyed faithfully along the peripheral main trunk.[9,18] However, in a recent investigation, we demonstrated the presence of conduction failure (measured as a lack of action potentials along the axon in response to titanic stimulus) in nociceptive C-fibers in a manner that was significantly attenuated under conditions of hyperalgesia. This suggests that conduction failure may serve as an intrinsic self-inhibitory mechanism for the modulation of persistent nociceptive input along nociceptive C-fibers.[33,42] Targeting the factors involved in conduction failure might therefore represent a new therapeutic target for the treatment of abnormal peripheral pain.

Sponsorships or competing interests that may be relevant to content are disclosed at the end of this article.

[a] Department of Neurobiology and Collaborative Innovation Center for Brain Science, School of Basic Medicine, Fourth Military Medical University, Xi'an, China, [b] Department of Psychology, Fourth Military Medical University, Xi'an, China, [c] Department of Cardiology, Xjing Hospital, Fourth Military Medical University, Xi'an, China, [d] Britton Chance Center for Biomedical Photonics, Wuhan National Laboratory for Optoelectronics, Huazhong University of Science and Technology, Wuhan, China, [e] The 323 Military Hospital, Xi'an, China, [f] Department of Radiation Biology, Faculty of Preventive Medicine, Fourth Military Medical University, Xi'an, China

**Corresponding author. Address: Department of Neurobiology and Collaborative Innovation Center for Brain Science, School of Basic Medicine, The Fourth Military Medical University, 169# Changle West Rd, Xi'an 710032, China. Tel.: 86 29 84774564-802; fax: 86 29 83246270. E-mail address: xingjunl@fmmu.edu.cn (J. Xing).*

Supplemental digital content is available for this article. Direct URL citations appear in the printed text and are provided in the HTML and PDF versions of this article on the journal's Web site (www.painjournalonline.com).

PAIN 157 (2016) 2235–2247

http://dx.doi.org/10.1097/j.pain.0000000000000632

In the last decade, new findings suggest that hyperpolarization-activated, cyclic nucleotide–modulated (HCN) channels are widely distributed on nociceptors.[2,14,26] Increases in current mediated by HCN2 channels (I_h) play a pivotal role as a pacemaker for nociceptive signals in both inflammatory and neuropathic pain states.[4,13,29,30,37] ZD7288, an HCN channel antagonist that decreases I_h current, alleviates nociceptive responses and produces significant analgesia in a variety of classical pain models.[4,13,27,28] However, systemic therapeutic administration of such a pan-HCN antagonist is limited by off-target effects such as bradycardia mediated by the inhibition of HCN4 in the sinoatrial node.[23,25] In a previous study, we found that the application of ZD7288 to normal peripheral nerve markedly enhanced the degree of conduction failure along the main axon of C-fibers.[42] In this study, we investigated the ability of local ZD7288 administration to produce effective C-fiber conduction failure and analgesia in the absence of side effects classically associated with analgesic therapy.

2. Materials and methods

2.1. Animals

The animals were obtained from the Animal Center of the Fourth Military Medical University and were handled and cared for in accordance with the Guide for United States Public Health Service's Policy on Humane Care and Use of Laboratory Animals. The protocol was approved by the Committee on the Ethics of Animal Experiments of the Fourth Military Medical University. All efforts were made to minimize animal suffering and the number of animals used.

2.2. Inflammatory pain model

Subcutaneous injection of complete Freund's adjuvant (CFA) is a model of inflammatory pain that is primarily mediated by C-fibers; accordingly, we used this model to observe alterations in C-fiber conduction. Complete Freund's adjuvant (10 μL; Sigma-Aldrich, St. Louis, MO) was injected subcutaneously into the distal third of the tail under diethyl ether anesthesia or intradermally into the unilateral hind limb. In the latter model, 2 sites within the cutaneous receptive fields of the L4 and L5 dorsal root ganglia (DRG) were injected simultaneously: one into the plantar surface of the left hind paw and the other into the dermis lateral to the left knee. This induced edema of the entire hind limb as previously described.[11] In imaging experiments, an identical CFA model (into the unilateral hind limb) was used in mice.

2.3. In vivo single-fiber recording

In vivo single-fiber recordings were performed in adult male and female Sprague-Dawley rats (150-200 g). Recordings were obtained from a single polymodal nociceptive C-fiber of the coccygeal nerve. For this procedure, the nerve was exposed at 2 sites. The proximal site was used for single C-fiber recording, and the distal site was used for drug administration to the nerve trunk. The receptive field of the single polymodal nociceptive C-fiber was identified with both mechanical and thermal stimuli as previously described[21,31] and 2 stimulus electrodes were inserted into the skin for electrical stimulus delivery. When a polymodal nociceptive C-fiber was identified, the degree of conduction failure was measured using repetitive electrical pulse stimuli (1.5 millisecond duration, 120% threshold intensity) in different frequencies (2, 5, and 10 Hz) for 60 seconds.[33,42] The degree of conduction failure was calculated as the ratio of the number of failures (nonresponses to repetitive stimulus pulses) to the total number of delivered repetitive stimulus pulses multiplied by 100.

During recording, the ipsilateral coccygeal nerve was exposed at the proximal region of the tail. The nerve filaments were dissected from the intact nerve under warm mineral oil, and the distal ends were placed on a fine platinum electrode for distinguishing and recording polymodal nociceptive C-fiber afferent firings. The stimulus electrode was inserted into the skin of the identified receptive field, stimuli were delivered to the coccygeal nerve, and conduction velocity (CV) was measured. The nerve fibers were categorized based on axon CV as C (<2 m/s), A_δ (2-12 m/s), or A_β (>12 m/s). To distinguish between a failure to evoke an action potential and a conduction failure, the following steps were carried out. First, to avoid anodal blockade (blockade of impulse propagation induced by repetitive electrical stimuli), the anode electrode was placed at a position distant from the recording site. Moreover, the stimulus intensity used was 120% threshold of the recorded C-fiber. Second, since it is impossible to record from 2 different sites on the same fiber, as the fine filament containing the single fiber must be dissected at the recording location, we arranged 2 pairs of stimulating electrodes along the main nerve trunk with different distances from the recording electrode. Using the same stimulus parameters, a greater degree of conduction failure was observed for longer distance propagation than that in the shorter distance propagation, suggesting failure of the conduction process. The chemicals were applied to a bath located between the stimulus and recording areas to deliver drugs to the axons within nerve trunk. The initial CV (CVi) and CV slowing (CVS) were termed and detected according to the description given previously.[17,36,42] The CV of the first evoked action potential was defined as the CVi, and the CVS was calculated by the difference between the first CVi and last CV of a firing train as a percentage of CVi.

2.4. In vitro patch clamp recordings from dorsal root ganglion neurons

On days 3 to 7 after CFA injection, the L4 and L5 DRG with the attached sciatic nerve were carefully dissected in anesthetized animals for in vitro electrophysiological analysis. The connective tissue was removed, and the DRG capsule was excised using 2 fine-tipped tweezers under the stereoscope. The preparation was then digested at 37°C with a mixture of 0.4 mg/mL trypsin (Sigma-Aldrich) and 1.0 mg/mL type-A collagenase (Sigma-Aldrich) for 30 minutes. The intact ganglia were then incubated in artificial cerebrospinal fluid (content in mM: NaCl 125, KCl 3.8, NaH_2PO_4 1.2, $NaHCO_3$ 26, glucose 10, $MgCl_2$1.0, $CaCl_2$ 2.0, pH 7.2, osmolarity 300 mOsm) oxygenated with 95% O_2 and 5% CO_2 at 28°C for at least 1 hour before transferring to the recording chamber. Whole ganglia were individually stabilized using a slice anchor, and nerves were connected to a suction-stimulating electrode.

Dorsal root ganglion neurons were visualized with a 40× water-immersion objective, using a microscope (BX51WI; Olympus, Tokyo, Japan) equipped with infrared differential interference contrast optics. Neuronal activity was recorded at room temperature (23°C) in whole-cell current and voltage mode, using a Multiclamp 700B amplifier (Molecular Devices Corporation, Sunnyvale, CA). Patch pipettes were pulled from borosilicate glass capillaries on a puller (Model P-97; Sutter Instrument CO, Novato, CA). The electrode had a final resistance of 4 to 7 MΩ when filled with normal pipette solution containing (in mM): 120 potassium gluconate, 18 KCl, 2 $MgCl_2$, 5 EGTA, 10 HEPES, 5 Na_2-ATP, 0.4 Na-GTP, and 1 $CaCl_2$ (pH 7.2 adjusted with KOH, osmolarity 300 mOsm). All chemicals were purchased from Sigma (St. Louis, MO) unless otherwise indicated. Pipette offset current was zeroed immediately prior to contact with the cell membrane, and the electrode capacitance was canceled after the establishment of

a gigaohm seal. The series resistance was 10 to 30 MΩ. After establishing whole-cell recording mode, the series resistance was compensated to 70% to 75%.

Five stimulus protocols were used to detect the response of DRG neurons. First, a series of 400-millisecond depolarizing currents (0.1-2.5 nA in increments of 0.1 nA) were injected to elicit action potential; second, repetitive discharges of 5 to 50 Hz were delivered to the sciatic nerve through the suction electrode to screen for conduction failure; third, alternatively, a train of 200 pulses (with a duration of 1-2.5 millisecond duration, 120% threshold intensity) were delivered intracellularly to detect conduction failure; fourth, hyperpolarizing step currents were injected in current clamp mode to determine whether the "sag" and "rebound" action potential could be induced; fifth, hyperpolarizing potentials between −130 and −60 mV were delivered in increments of 10 mV from a holding potential of −60 mV for a duration of 6 seconds to activate I_h. I_h was subsequently obtained by subtracting the initial current from the resultant steady-state current.[32] Neurons were selected for further study if they had a resting membrane potential greater than −50 mV and if they exhibited overshooting action potentials. The after-hyperpolarization potential (AHP) amplitude was measured from baseline to peak, and the 80% AHP duration was measured as an interval from the onset of the AHP to the point of 80% decay.[12,15]

Data were acquired with a Digidata 1322A acquisition system (Molecular Devices) using pCLAMP 9.0 software. Signals were sampled at 10 kHz and analyzed offline. Final data were processed using Origin 8.0 and Visio 2003 software.

2.5. Calcium imaging as a measure of activity of dorsal root ganglion soma

Electrophysiological recording and fluorescence imaging were performed simultaneously in the DRG soma of Thy1-GCaMP3 transgenic mice. Corresponding experiments were carried out in these mice in a self-prepared chamber with 3 baths and preparation of DRG with attached peripheral sciatic nerves. The 3 compartments were isolated both chemically and electrically and connected to the neighboring by either a hole or a groove. After the preparation was mounted, petroleum jelly was used to fill the interspace of either the hole or the groove. Recordings were performed at room temperature in oxygenated artificial cerebrospinal fluid and with normal pipette solution as described above. Cells were recorded in current-clamp mode and repetitive discharges of 5 to 20 Hz (500 μs duration, 1-5 mA intensity) were delivered to the sciatic nerve through the suction electrode to induce action potentials that would propagate towards DRG somata. Imaging was performed using a fluorescence microscope (BX 51W1; Olympus) equipped with a Xenon lamp and a monochromator from Polychrome V (Till Instrument) which is an ultrafast switching monochromator with a fully digital high precision galvanometer-driven grating. Light with a wavelength of 488 nm was used for excitation, and fluorescence was recorded through a band-pass filter of 505 to 525 nm. Images were acquired using a 40× water-immersion objective with a 5-Hz scanning speed. The average fluorescence intensity in the soma was measured by Metafluo data processing software and analyzed using MATLAB software. Fluorescence changes over time is reported as $\Delta F/F = ([F - F_B] - [F_0 - F_B])/(F_0 - F_B)$, in which F is the raw fluorescence signal, F_B is the background signal, and F_0 is the mean fluorescence signal determined during a baseline period prior to the action potential stimuli.[5] For drug application, a segment of the sciatic nerve was isolated in a small liquid bath by mounting at the 2 ends of the nerve.

2.6. Immunofluorescence labeling

On days 3 to 7 after CFA injection, rats were anesthetized with pentobarbital sodium and transcardially perfused with saline followed by 4% paraformaldehyde. Dorsal root ganglia from the lumbar regions of the spinal column and coccygeal nerves were harvested, postfixed overnight in 4% paraformaldehyde, and cryoprotected in 30% sucrose at 4°C until the tissue density exceeded that of the cryoprotection medium. Transverse DRG sections (15 μm thick) and sagittal coccygeal nerve sections (12 μm thick) were cut on a freezing microtome. To visualize HCN channels, double immunofluorescence labeling methods were used. In brief, sections were incubated with a solution containing 0.3% Triton X-100 and 1% bovine serum albumin for 3 hours at room temperature. Sections were then incubated with anti-HCN1 (1:200; Almone Labs, Jerusalem, Israel) or anti-HCN2 (1:200; Almone Labs) and anti-peripherin (1:1000; Sigma-Aldrich) in phosphate-buffered saline containing 0.5% Tween 80 (PBS-T) for 24 hours at 4°C. After 3 washes with PBS-T, sections were incubated with Alexa Fluor 488 and Alexa Fluor 594 secondary antibodies (Molecular Probes) for 2 hours at room temperature. For each animal, 3 sections were randomly selected and imaged with an Olympus confocal microscope. The density threshold was measured by averaging the density of 3 neurons in one section, which was determined to be minimally positive with ImageJ software. All neurons for which the mean density exceeded the threshold >25% were judged to be positive. Positive cells were determined as the percentage of total counted DRG neurons. Only neurons that were positively classified in 2 individual images were categorized to coexpress the 2 target proteins. All images were then processed with Adobe Photoshop software.

2.7. Western blot

Dorsal root ganglia and coccygeal nerves were collected and homogenized in ice-cold lysis buffer containing (in mM): Tris-HCl, pH 7.4, 150 NaCl, 5 EDTA, 1% Triton X-100, 0.5% sodium deoxycholate, 0.1% sodium dodecyl sulphate, and standard protease inhibitors. Insoluble materials were removed by centrifugation (13,000 rpm, 10 minutes), and supernatants were collected for analysis. The protein concentration for each sample was determined by the bicinchoninic acid method using the MICROBCA protein assay kit (Pierce). Proteins were separated on a gel and subsequently transferred to a membrane. Membrane blots were blocked with 10% non-fat dry milk for 12 hours, incubated with primary antibodies (anti-HCN1, 1:100 and anti-HCN2, 1:100) overnight at 4°C and finally incubated with an appropriate horseradish peroxidase–conjugated secondary antibody (1:10,000; Amersham Biosciences, Pittsburgh, PA) for 2 hours at room temperature. To normalize the loaded samples, anti-actin antibody (1:5000, GE Healthcare) and an appropriate horseradish peroxidase–conjugated secondary antibody (1:5000, Pierce) were used to identify β-actin as a loading control. For visualization, membranes were incubated with enhanced chemiluminescence reagents (Pierce), images were acquired with the CHEMIL-MAGER chemiluminescence imaging system, and bands were analyzed using ImageJ software. The density of each band of interest was measured and normalized to the density of the corresponding β-actin band.

2.8. Animal behavioral testing experiments

Behavioral experiments were conducted in a blinded fashion (ie, the experimenter was unaware of the experimental conditions). Mechanical allodynia and thermal hyperalgesia were measured

as previously described.[20,31] In brief, rats were placed in suspended individual chambers with mesh flooring and allowed to acclimate for 30 minutes. A series of calibrated von Frey filaments were applied perpendicularly to the central region of the glabrous surface of the hind paw in the order of increasing bending force from 0.6 to 26 g (Stoelting, Wood Dale, IL) for 5 seconds each and with 15-second intervals. Brisk withdrawal or paw flinching was considered to indicate a positive response. The threshold was defined as the force eliciting a 50% withdrawal. To measure thermal sensitivity, the latency for paw withdrawal from a radiating heat source with an automated device readout was measured (IITC Life Science Inc, Woodland Hills, CA). The time course (from 3 days before to 15 days after CFA injection) for the development of and recovery from CFA-induced mechanical allodynia and thermal hyperalgesia is provided (Supplementary Fig. 1, available online at http://links.lww.com/PAIN/A283). A stable allodynia and hyperalgesia during the 3 to 7 days after CFA injection was observed. Corresponding electrophysiological and immunofluorescence labeling experiments were performed within this period.

During the abovementioned assessments, motor function of the involved leg was assessed every 15 minutes as previously described[19]; in brief, animals were scored as following: 2, full paralysis; 1, partial paralysis; 0, no impairment. For drug administration, sciatic perineuronal injections were carried out as previously described.[3,34] In brief, the ischial tuberosity and the greater trochanter were localized by palpation. On an imaginary line between these 2 landmarks and about one-third of the distance caudal to the greater trochanter, a 27-G needle was advanced at a 45° angle from dorsal lateral direction until the tip encountered the ischium. Then a 200 μL volume of either ZD7288 or saline was injected.

Furthermore, in the formalin test, the late phase was considered to be related to the activity of C-fibers. The mean time spent on behaviors was 0 to 10 minutes for the early phase and 15 to 60 minutes for the late phase.

2.9. Statistics

Data are presented as the mean ± SEM and were analyzed using either an analysis of variance or a 2-tailed Student *t* test. The level of significance was set at $P < 0.05$.

3. Results

3.1. ZD7288 enhances the degree of conduction failure in nociceptive C-fibers under an inflammatory condition

All of the following investigations were based on the assumption that conduction failure is a common occurrence along nociceptive C-fibers, which is supported by the results of our previous investigations.[33,41,42] Whereas C-fiber conduction failure can be observed in normal animals, decreases in conduction failure occur under conditions of notable hyperalgesia, such as painful diabetic neuropathy.[33] In this study, further investigations in an inflammatory pain model were carried out. After the establishment of CFA-induced mechanical allodynia and thermal hyperalgesia, we recorded activity from single polymodal nociceptive C-fibers of the coccygeal nerve activated by a stimulating electrode positioned over the receptive field (Supplemental Fig. 2A, available online at http://links.lww.com/PAIN/A283). After CFA injection into the tail, the degree of frequency-dependent conduction failure was reduced significantly relative to control (Supplemental Figs. 2B–D, available online at http://links.lww.com/PAIN/A283). These data suggest that the conduction failure of pain-relevant polymodal nociceptive C-fibers is attenuated in the CFA model of inflammatory pain.

We next examined the effect of local ZD7288 administration on attenuated polymodal nociceptive C-fiber conduction failure in the CFA model. ZD7288 dose-dependently increased CVS and the degree of conduction failure in CFA model rats (**Fig. 1A**). We also observed a dose-dependent increase in the dispersion of interspike interval (ISI) series distributions (**Fig. 1A**, bottom). Furthermore, spontaneous firing activity is considered to be a surrogate indicator of spontaneous pain and was observed in 20% of polymodal nociceptive C-fibers in CFA model rats. The application of ZD7288 decreased this spontaneous firing activity in a dose-dependent manner (Supplemental Fig. 3, available online at http://links.lww.com/PAIN/A283), indicating a potential effect on spontaneous pain.

The effect of ZD7288 on conduction failure had 2 distinct features. One feature was activity dependence, ie, higher frequencies of afferent signaling uncovered greater effects of ZD7288 on the degree of conduction failure (**Fig. 1B**). The second feature was the dependence on the type of nerve fiber. After application of 150 μM ZD7288 to the nerve trunk, the degree of both CVS and conduction failure increased in C-fibers, while little-to-no effect was observed in A-fibers (**Fig. 1C**). Furthermore, ZD7288 had no effect on A-fibers at a dose range of 50 to 250 μM in response to stimulus frequencies below 20 Hz (0 of 23 fibers, 19 Aβ fibers, and 4 Aδ fibers).

3.2. ZD7288 selectively enhances conduction failure at the level of the dorsal root ganglia

To further confirm the selectivity of the effect of ZD7288 on C-fiber conduction failure in primary sensory neurons, conduction failure was evaluated using fluorescent imaging of DRG neurons from Thy1-GCaMP3 transgenic mice.[5] This experiment was based on the idea that genetically encoded calcium indicators are a powerful tool for mapping neuronal activity without causing significant neuronal damage.[1,5,6] For these studies, we used a preparation of DRG with attached peripheral nerves (**Fig. 2A**). First, we confirmed the expression of GCaMP protein in the DRG somata of both small- (<20 μm) and large- (>50 μm) diameter neurons. We then performed whole-cell patch recording and imaged changes in fluorescence simultaneously. A single action potential evoked detectable calcium transients with average ΔF/F amplitudes of 5% (**Fig. 2B**). Moreover, the amplitude of fluorescence changes correlated well with the number of observed spikes (**Fig. 2C**).

Following these baseline studies, the effect of ZD7288 was examined. During the electrical stimulation of afferent nerves (5 Hz for 40 seconds), both small-diameter and large-diameter neurons in the DRG exhibited rapid increases in fluorescence intensity. Administration of ZD7288 (50 μM) to the nerve trunk (**Fig. 2A**) produced a remarkable decrease in the peak fluorescence intensity of small-diameter neurons (peak value 54.6 ± 16.9%, n = 20) but had little-to-no effect on large-diameter neurons (17.1 ± 6.2%, n = 27; **Fig. 2D**). These results demonstrate that local application of ZD7288 to afferent nerves selectively enhances the degree of conduction failure in nociceptive small-diameter neurons, but not in large-diameter neurons.

3.3. ZD7288 promotes conduction failure by reducing the rising slope of the after-hyperpolarization potential in small-diameter dorsal root ganglion neurons

We next investigated the mechanism of ZD7288-mediated conduction failure. At present, it is technically difficult to directly patch clamp C-fibers; therefore, we measured the relationship between conduction failure and changes in membrane potential

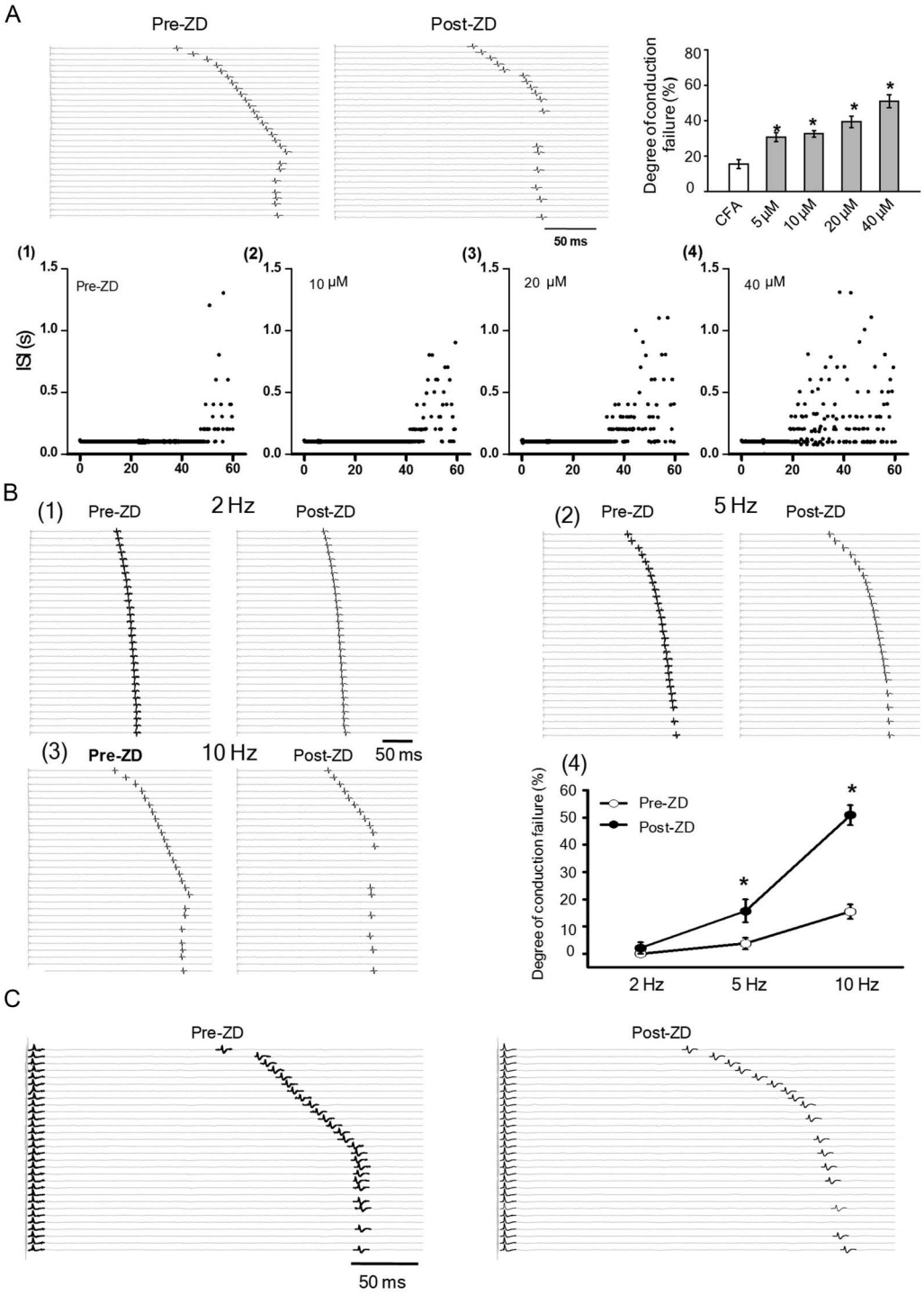

Figure 1. Effects of ZD7288 on conduction failure of C-fibers in CFA model. (A) Upper left 2 panels: ZD7288 application (40 μM, Post-ZD) enhanced conduction failure in polymodal C-fiber relative to control (Pre-ZD). Every 20th sweep is shown (consecutive sweeps were at 2-second intervals) and is displayed top-to-bottom (similar as below). Upper right: Dose–response histograms for the effect of ZD7288 on conduction failure (n = 12). Bottom: representative change in the inter-spike interval (ISI) during repetitive stimulation before and after ZD7288 application. (1) ISI from a series of discharges evoked by 10-Hz repetitive stimulation of a single C-fiber from a complete Freund's adjuvant—injected rat. Increase and scatter of ISI series started at about 45 seconds, indicating conduction failure has occurred. (2-4) Change of ISI for the same C-fiber after the application of varying concentrations of ZD7288 (10 μM, 20 μM, or 40 μM), note the earlier appearance of the ISI series change along with the increase of the concentration of ZD7288, indicating that the degree of conduction failure was enhanced in a concentration-dependent manner. (B) (1) original consecutive recordings of single C-fiber activity in response to electrical stimulation (2 Hz) of the receptive field before (left) and after (right) ZD7288 application (40 μM). (2) The same recordings performed in response to 5-Hz stimulation. (3) The same recordings performed in response to 10-Hz stimulation. (4) ZD7288 enhanced the conduction failure of C-fibers in an activity-dependent manner (n = 8). (C) ZD7288 selectively enhanced the conduction failure on polymodal C-fiber (with longer latency) but not on A-fiber activity (with shorter latency). *$P < 0.05$ vs control.

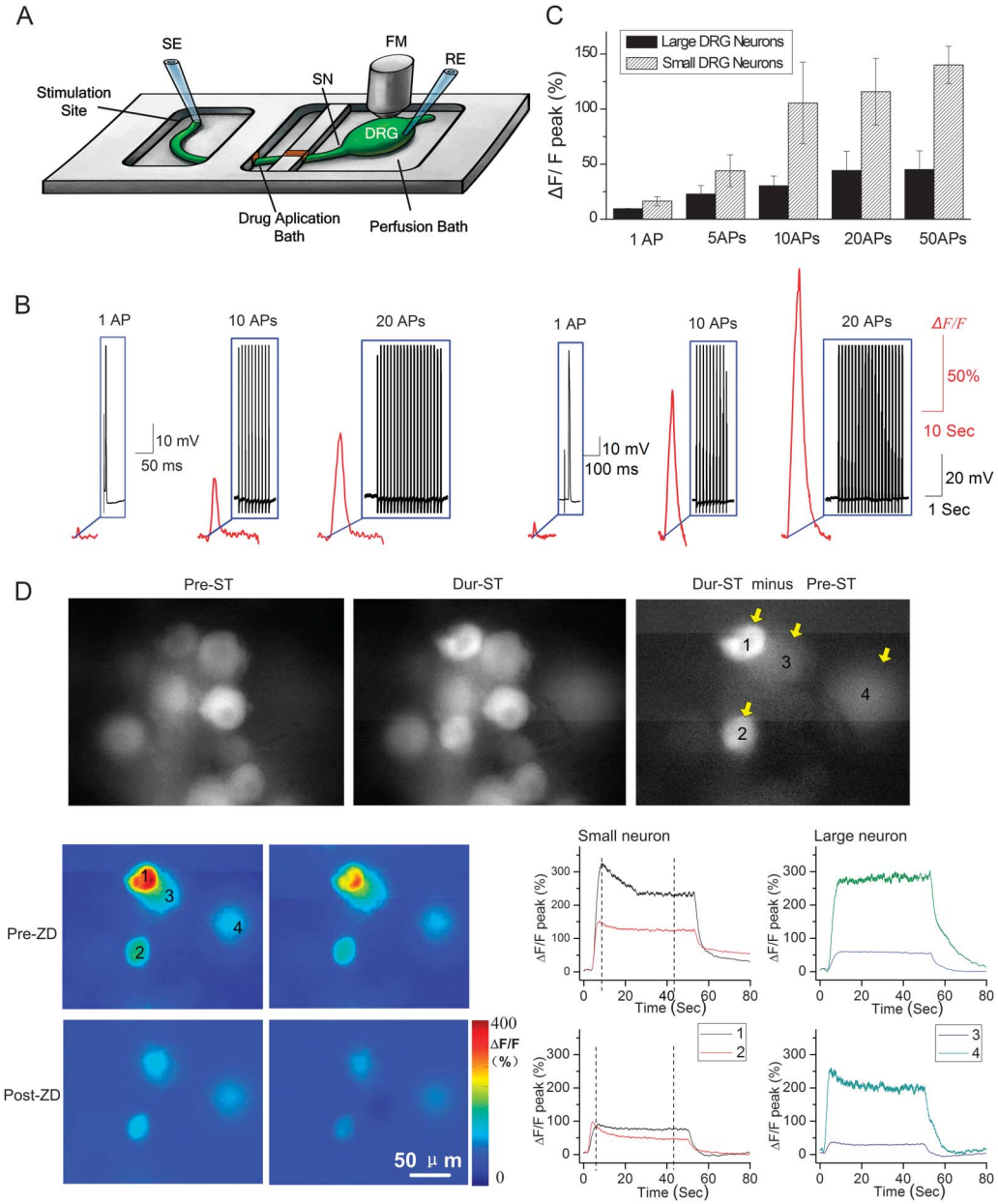

Figure 2. C-fiber conduction failure at the level of the DRG in Thy1-GCaMP3 transgenic mice. (A) The experimental scheme for simultaneous patch-clamp recording and fluorescence imaging of DRG. Dorsal root ganglia with attached peripheral sciatic nerves were prepared. There were 3 isolated baths: one for DRG perfusion, one for ZD7288 application, and one for electrical stimulation of the sciatic nerve with a suction electrode. (B) Representative ΔF/F traces (red) for different numbers of action potentials across large-diameter (left panel) and small-diameter (right panel) DRG neurons from Thy1-GCaMP3 mice. Insets show the evoked spikes for each cell. (C) Fluorescence responses increased in tandem with increases in the number of spikes for both large-diameter and small-diameter DRG neurons (n = 9). (D) Fluorescence change as a surrogate for conduction failure was measured in 2 large-diameter and 2 small-diameter DRG neurons via stimulation with 200 spikes (5 Hz, 40-second duration). Upper: fluorescence images of the baseline response (Pre-ST), the response to stimulation (Dur-ST), and the difference between the Pre-ST and Dur-ST responses (Dur-ST minus Pre-ST), respectively. Minor fluorescence changes were observed in large- (3, 4) vs small- (1, 2) diameter DRG neurons before (middle images and traces) and after (bottom images and traces) ZD7288 application. The color image was obtained at the time point marked by the vertical dashed line in the left panel trace. DRG, dorsal root ganglion; RE, recording electrode; SE, stimulation electrode; FM, fluorescence microscope; SN, sciatic nerve.

for small-diameter DRG neurons. In this study, conduction failure was reflected by spike failure in response to repetitive stimulus pulses. We focused on the AHP because it is noticed that some thin axons became hyperpolarized when the spike activity exceeded 1 to 5 Hz.[30] In response to single pulse stimulation, the 80% AHP recovery time in small-diameter neurons (149.2 ± 12.6 millisecond, n = 26) was significantly longer than that in large-diameter neurons (17.0 ± 2.2 millisecond, n = 10) (**Figs. 3A and C**). Following repeated stimuli at a lower frequency (5 Hz), the 80% AHP recovery time measured from the last spike of the stimulus series was significantly prolonged in small-diameter neurons according to the spike number (**Figs. 3B and D**). Further examination revealed that, within the stimulus series, spikes in response to repetitive stimuli could pile up on the previous AHP and led to a reduction in the rising slope of the following AHP (**Figs. 3E and F**). Therefore, the observed reduction in the rising slope of the AHP primarily reflected the prolongation of the AHP within the repetitive firing instead of 80% AHP recovery time. This

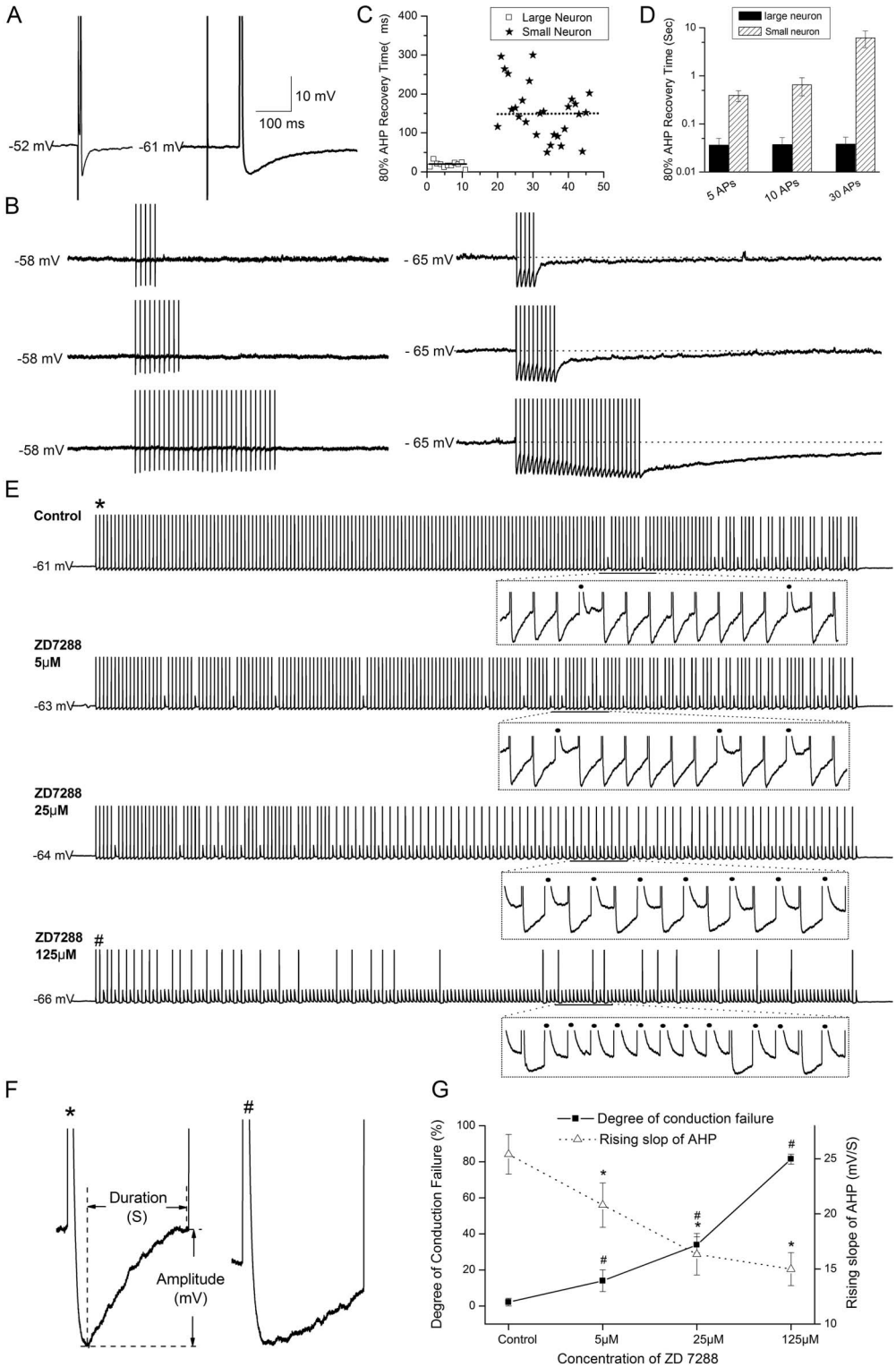

Figure 3. ZD7288 enhances the conduction failure of small-diameter DRG neurons by decreasing the rising slope of the AHP. (A) Traces demonstrating representative AHPs for large-diameter (left) and small-diameter (right) DRG neurons in response to peripheral sciatic nerve stimulation. The conduction velocity of each neuron was calculated from the latency (21.43 and 0.33 m/s for large- and small-diameter neurons, respectively). (B) Change in AHP for the last spike in response to repetitive stimulation (5 Hz) in large-diameter (left panel) and small-diameter DRG neurons (right panel). The AHP of small-diameter neurons was prolonged in a manner proportional to stimulation. (C) Scatter plot showing the distribution of 80% AHP recovery times for large- and small-diameter DRG neurons. The average time is marked by a dotted line for small-diameter neurons and by a solid line for large-diameter neurons. (D) Statistical comparison of 80% AHP recovery times for large- and small-diameter DRG neurons. (E) Continuous recordings of series firing responses to 5-Hz stimulation under control conditions or in the presence of varying concentrations of ZD7288 in a small-diameter DRG neuron from a complete Freund's adjuvant–injected rat. Insets show expanded traces for the specified intervals. Dark spots represent spike failures. (F) Representative traces used to measure the rising slope of the AHP. The rising slope was equal to the amplitude difference between the maximum and minimum AHP voltages (mV) divided by duration (interval of stimuli, in seconds). The left panel illustrates a larger rising slope (from the first trace in panel E marked with "*"), and the right panel shows a smaller rising slope (from the fourth trace in panel E marked with "#") after ZD7288 application (125 μM). (G) Relationship between the degree of conduction failure and the rising slope of the AHP in response to different concentrations of ZD7288 (n = 4). * and #$P < 0.05$ vs control. AHP, after-hyperpolarization potential.

was consistent with the fact that after repeated intracellular short-pulse stimulation (a train of 200 pulses, 5 Hz, 1-2.5 millisecond duration, 120% threshold), the rising slope declined from 41.42 to 30.25 mV/s (**Fig. 3E**, first trace). Using this parameter, we uncovered a negative correlation between spike failure and AHP alteration within the repetitive activities (**Fig. 3G**). Of note, these effects in response to lower frequency stimulation were not observed in large-diameter neurons (**Fig. 3B**).

Next, we examined the effect of ZD7288 on spike failure. After the local application of different concentrations of ZD7288, 2 results were observed (**Fig. 3E**). In the first result, 3 types of spike failure occurred: (1) one in which the failure appeared sporadically; (2) one in which firing and failure appeared alternately, and failure always presented at the point of greater hyperpolarization; and (3) one in which several failures appeared continuously at time points with a smaller rising slope of the AHP or a greater hyperpolarization potential. The second result was that activity-dependent decreases in the rising slope of the AHP were further reduced from 20.80 ± 2.01 to 14.99 ± 1.51 mV/S and was accompanied by an enhanced degree of spike failure (**Figs. 3E and G**). These results suggest that a reduction in I_h is correlated with the decrease of the rising slope of the AHP and then led to the augmentation of spike failure. These results might partially reveal the dynamic relationship between the conduction failure and the changes in AHP along nociceptive C-fibers. While, in large-diameter DRG neurons (>50 μm), repeated stimulation between 5 to 50 Hz did not evoke any piling up of the AHP because of its short-duration property. So, even with a relative larger I_h current density compared with those in small-diameter DRG neurons of CFA-injected animals (Supplemental Figs. 4C and D and Fig. 5C, available online at http://links.lww.com/PAIN/A283), the only changes were the hyperpolarization of the membrane potential (−60.1 ± 5.4 mV vs −64.0 ± 6.1 mV) and thus a decreased AHP amplitude (9.2 ± 1.7 mV vs 5.4 ± 1.8 mV, n = 12) in response to the ZD7288 application, but no change of the conduction failure (Supplemental Figs. 4A and B, available online at http://links.lww.com/PAIN/A283).

3.4. Alterations in ionic channel function underlie the effect of ZD7288 on C-fiber conduction

Given the significant effect of ZD7288 on the conduction failure of nociceptive C-fibers as well as on the AHP activity of small-diameter DRG neurons in CFA model animals, we next examined the expression of HCN channels in the coccygeal nerve and on DRG soma. We first evaluated HCN2 as it has been explored as an analgesic therapeutic target in a variety of animal models.[13,14,28,29] As expected, the expression of HCN2 was increased in both the coccygeal nerve and small DRG neurons in CFA-injected rats relative to control rats (**Figs. 4A and C**). Confocal analysis of the double immunofluorescence revealed that the intensity of HCN2 immunoreactivity and the percentage of HCN2-positive cells were significantly increased in CFA-injected rats (**Figs. 4B and D**). Furthermore, Western blottings

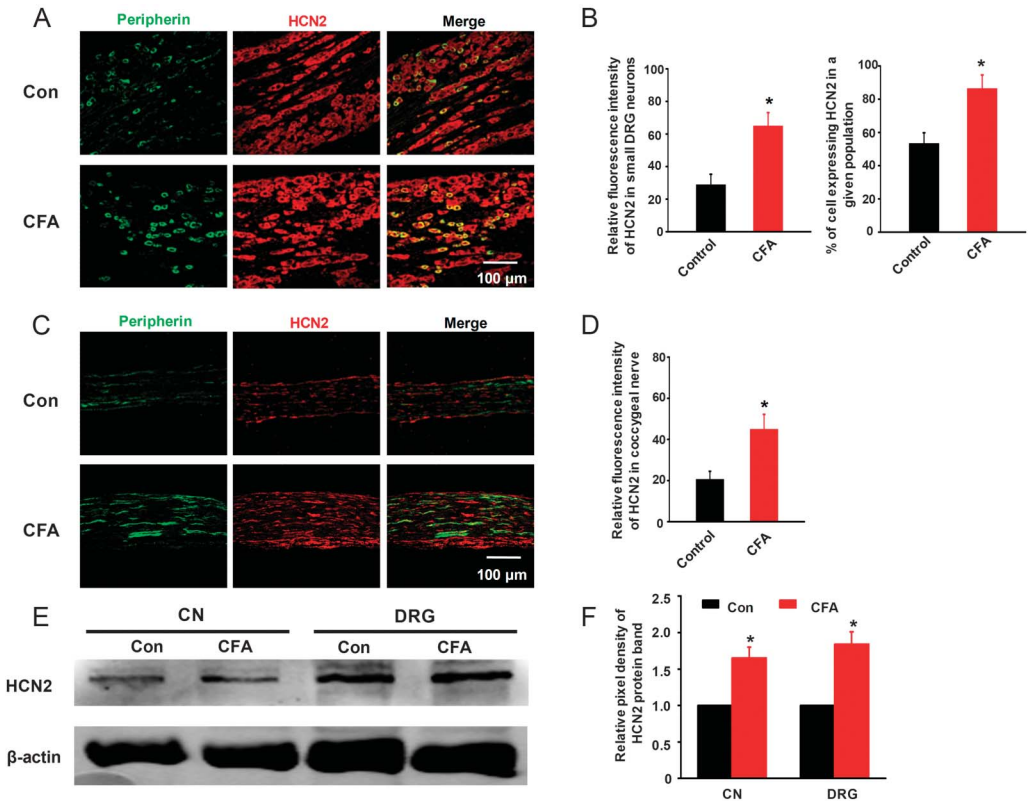

Figure 4. HCN2 expression is increased in the DRG and coccygeal nerves of CFA-injected rats. (A) Representative images of DRG neurons double-labeled for HCN2 (red) and peripherin (green). (B) Left: quantitative analysis of HCN2 fluorescence intensity in small-diameter DRG neurons from control and CFA-injected rats. Right: percentages of HCN2-positive cells in DRG tissues from control (n = 5) and CFA-injected (n = 6) rats. (C) Representative images of coccygeal nerves double-labeled for HCN2 (red) and peripherin (green). (D) Quantitative analysis of HCN2 fluorescence intensity in coccygeal nerve tissues from control and CFA-injected rats (n = 6). (E) HCN2 expression in DRG and coccygeal nerves from control and CFA-injected rats. (F) Quantitative analysis of the Western blotting data represented in panel E. All data are represented as the mean ± SEM. *$P < 0.05$ vs the control group. CFA, complete Freund's adjuvant; Con, control; CN, coccygeal nerve; DRG, dorsal root ganglion.

showed that expressions of HCN2 were also significantly increased in DRG and coccygeal nerves derived from CFA-injected rats compared with control rats (**Figs. 4E and F**). Similarly, increased expression of HCN1 channels was also found in the CFA-injected coccygeal nerve and DRG small neurons compared with the control group (Supplemental Fig. 5, available online at http://links.lww.com/PAIN/A283). These changes in expression highlight a possible target for the action of ZD7288. In agreement with HCN2 as a hypothesized target, the sag component and amplitude of I_h current were increased in DRG small-diameter neurons isolated from CFA-injected rats, and this effect was inhibited by the application of ZD7288 (**Fig. 5**).

3.5. Perineuronal injection of ZD7288 ameliorates inflammatory pain behaviors

Considering the effects of ZD7288 on the conduction failure of nociceptive C-fibers, we next evaluated the impact of local (perisciatic) injection of ZD7288[7,22] on CFA- and formalin-evoked pain behaviors in rats. ZD7288 significantly alleviated mechanical allodynia and thermal hyperalgesia in a dose-dependent manner (**Fig. 6A**). Furthermore, ZD7288 showed efficacy in the late phase but not the early phase of the formalin test (**Fig. 6B**), indicating that ZD7288 selectively inhibited the nociceptive activity of C-fibers in response to inflammatory pain.

As an analgesic agent, ZD7288 is limited by the side effects associated with systemic delivery.[4,23] Of note, a significant analgesic effect was achieved without motor deficits after the perineuronal injection of ZD7288 (up to 500 μM) (**Fig. 6C**), whereas perineuronal injection of lidocaine (0.2% or 2%) produced motor deficits in accordance with previous reports.[3] Intraperitoneal injection of ZD7288 (4 mg/kg) led to bradycardia (a reduction in heart rate from 300 to 200 beats/min) (**Fig. 6D**), consistent with the reported side effects after the intravenous injection of ZD7288.[4,23] In contrast, perineuronal injection (up to 500 μM) had no significant effects on cardiac rhythm (**Fig. 6D**). These results show that perineuronal injection of ZD7288 produces a reversal of mechanical allodynia and thermal hyperalgesia in the absence of observable bradycardia or motor deficits.

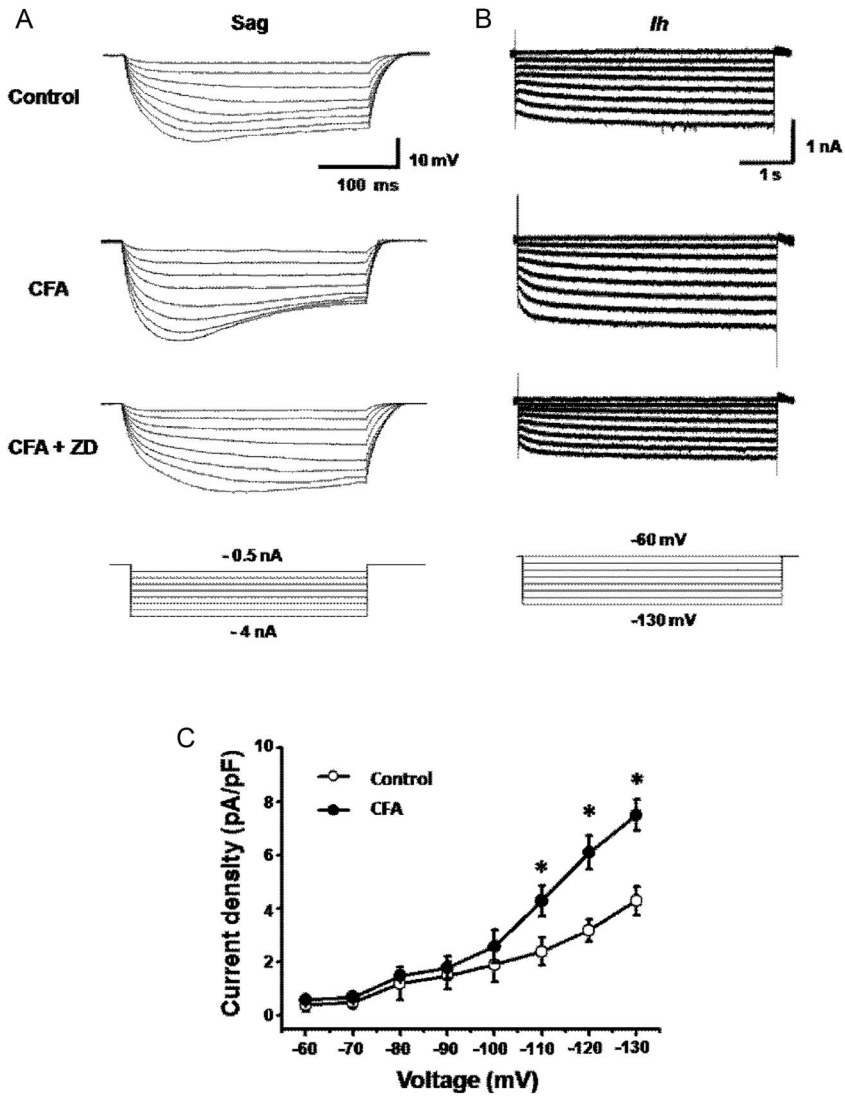

Figure 5. Complete Freund's adjuvant (CFA)-induced inflammation increases the hyperpolarization-activated cation current (I_h) in small-diameter DRG neurons. (A) Voltage sag of the membrane potential evoked by a series of hyperpolarizing current injections in small-diameter DRG neurons. (B) Representative I_h traces evoked by a series of hyperpolarizing voltage steps (bottom panel) from a holding potential of −60 to −130 mV for 6 seconds in 10 mV increments. (C) The mean current density of I_h in small-diameter DRG neurons from control and CFA-injected rats (n = 12). *$P < 0.05$ vs the control group.

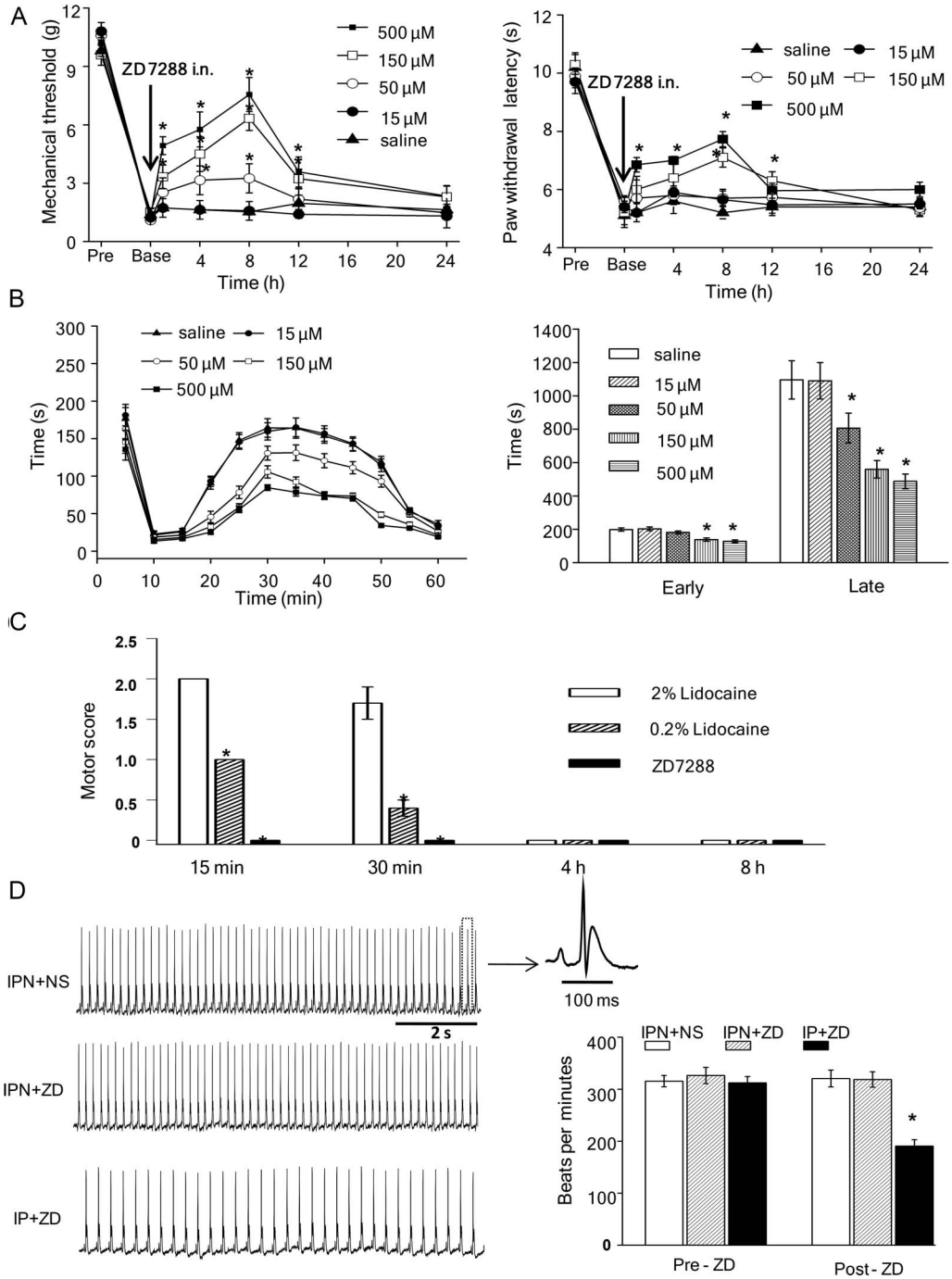

Figure 6. Perineuronal injection of ZD7288 alleviates pain behaviors in the absence of significant motor and cardiovascular side effects. (A) ZD7288 attenuated CFA-induced mechanical allodynia (left) and thermal hyperalgesia (right) in a dose-dependent and reversible manner (n = 15). In each figure, 3 days after CFA injection (the detection of mechanical threshold/paw withdrawal latency was indicated as Pre), rats received equivalent volumes of perineuronal saline or ZD7288 with different concentration after baseline assessment of tactile allodynia or hyperalgesia (indicated as Base). (B) Left: ZD7288 attenuated formalin-induced spontaneous flinching behaviors in a dose-dependent and reversible manner. Right: quantitative analysis of the effect of ZD7288 on spontaneous pain behaviors in the early and late phases of the formalin test (n = 6). (C) Comparison of the effects of perineuronal lidocaine (0.2% or 2%) and ZD7288 (500 μM) on motor function (n = 6). (D) Left: original heart rate recordings from rats after perineuronal saline injection (IPN + NS, top trace), perineuronal ZD7288 injection (500 μM, IPN + ZD, middle trace), or intraperitoneal ZD7288 injection (4 mg/kg, IP + ZD, lower trace) (n = 5). Right: quantitative analysis of the heart rate results are shown in panel D. *$P < 0.05$ vs the control group. CFA, complete Freund's adjuvant. IPN, perineuronal injection; NS, saline; ZD, ZD7288.

4. Discussion

The present investigation validates the results of a previous study reporting conduction failure along the main axon trunk of polymodal nociceptive C-fibers.[8] One of the fundamental features of conduction failure as observed in our study was activity- or frequency-dependence, such that higher stimulation frequencies produced greater degrees of conduction failure. It follows that higher intensity pain stimuli might also produce greater degrees of conduction failure as an intrinsic mechanism for modulating nociceptive input.[33,42] Under nonpathological circumstances, such an intrinsic self-inhibitory mechanism would serve to limit the extent of nociceptive signal propagation to the

central segment of the nerve and ultimately diminish the sensation of pain. Alternatively, reductions in conduction failure have been observed under pathological conditions such as in rodent painful diabetic neuropathy[33] as well as in the present study. Our results in models of inflammatory pain suggest that decreased self-inhibition elicited by inflammation or nerve injury could be a mechanism for alterations in pain sensation such as allodynia and hyperalgesia. Another vital feature of conduction failure in our study was its selectivity for C-fibers as opposed to A-fibers in response to stimulation frequencies between 0.5 and 50 Hz (**Fig. 1** and Supplemental Fig. 4, available online at http://links.lww.com/PAIN/A283). This hypothesis was supported by single-fiber recording and optical measurements in whole DRG mounts from Thy1-GCaMP3 transgenic mice. Taken together, conduction failure appears to be a frequency-dependent and C-fiber specific phenomenon that may serve as an intrinsic mechanism for limiting the sensation of pain.

The HCN antagonist ZD7288 also had a selective influence on C-fibers in the present study. Local administration of ZD7288 produced peripheral analgesia in a manner associated with the enhancement of conduction failure in C-fibers but not A-fibers. The effect of ZD7288 would be strongly supported by the detected facts of enhanced I_h current density and the expression of HCN channels. Inspired by Emery's investigation linking HCN2 function and signaling frequency in peripheral nerves,[13] we found that HCN2 expression was increased in small-diameter DRG neurons isolated from CFA-injected mice. The increase in both incidence and intensity provide support for the enhanced I_h current in CFA-injected animals. In addition, the expression of HCN1 was also increased, implying that an integrated expression of different HCN subtypes might contribute to the phenomenon of conduction failure. However, HCN1 was previously shown to be the main isoform expressed in large-diameter DRG neurons. It thus remains unclear why ZD7288 effects were absent in A-fiber conduction failure. The answer could be clarified only after the process of conduction failure was deeply explored and analyzed as discussed in the following section.

The exact mechanism of conduction failure remains elusive. In this study, we analyzed changes in membrane potential in small-vs large-diameter DRG neurons and observed a striking difference in AHPs between the 2 neuronal subtypes. Specifically, small-diameter DRG neurons displayed longer AHPs that were subject to piling up and summation within periods of repetitive firing, even in response to low frequency stimulation (ie, this reduced the rising slope of the AHP, increased the firing threshold and resulted in spike failure). Such changes increased along with the enhancement of stimulation frequency, displaying the features in the production of conduction failure—activity dependency. Conversely, much shorter AHPs were observed in large-diameter DRG neurons, and this prevented the piling up of AHP even in response to high frequency stimulation (50 Hz). These data suggest that large-diameter neurons are not vulnerable to spike failure in the same manner as small-diameter DRG neurons. In fact, previous studies have only identified A-fiber conduction failure at stimulation frequencies of 100 to 333 Hz or even higher and implicated Na^+ current in the observed mechanism.[35,38] Based on our observations, such high frequency stimulation would evoke rapid C-fiber failure and preclude the reliable configuration of conduction failure for experimental study. Rather, we selected a stimulation frequency ($<$50 Hz) that parallels the usually recorded input firing frequency for C-fibers. So, Wu and Henry's data suggest a sodium mechanism that underlies the conduction failure of large-diameter sensory neurons, whereas our study provides the original data for the essence of C-fiber conduction failure. In summary, the above findings reveal the dynamic relationship between changes in AHP and spike failure and, also, explain why the conduction failure selectively occurred on polymodal C-fibers.

In this study, after ZD7288 application, the piling up effect on the AHP and the production of conduction failure reinforced through further reducing the rising slope of AHP caused by blocking on I_h. Within this process, conduction failure exhibited different patterns, including sporadic, alternative, and continuous types (**Fig. 3**). It is important to note that ZD7288 can also block inward Na^+ currents[39] and T-type Ca^{2+} channels.[16] In our study, we compared the rising slope and the duration of the action potential (measured at half-width) before and after the application of ZD7288. There were some changes on these parameters, though the change of AHP was the most prominent. Recently, ivabradine was shown to be a more specific inhibitor of HCN channels–which lacks effects on Na^+, Ca^+, and K^+ currents.[40] Therefore, future studies using ivabradine can help delineate the exact contribution of I_h and other currents to AHP, conduction failure, and the adjustment of abnormal pain sensation.

A previous study focusing on A_β and A_δ fibers indicated that ZD7288 regulated I_h as a mechanism to block ectopic discharges but not conduction.[4] Rather than ascribing this observation to the off-target effects of ZD7288, a better explanation takes into consideration the roles of different cell and fiber types in different abnormal pain states. To this end, we observed an activity-dependent influence of ZD7288 on pain signals rather than a direct inhibitory action. This mechanism is in contrast to the effects of local anesthetics such as lidocaine,[22,29] which block ectopic firing by affecting Na^+ and K^+ channels. The above results also suggest that the AHP, especially in small DRG neurons, is an important target for modulating excitability and firing patterns. Any ionic current that contributes to the AHP of C-fiber could be involved in modulating conduction failure and therefore adjusting abnormal pain sensation. Though the AHP effect is not consistent with some other investigations in which the AHP was shortened in naïve neurons but not in axotomized neurons of myelinated fibers,[35] but still further, present results complement a different mechanism contributing to the neuropathic pain in which nociceptive C-fibers are involved.

Considering the important role of AHP in the production of conduction failure, it is easily understood why there is no effect of ZD7288 on A-fiber conduction failure with stimulation frequencies of less than 50 Hz. No matter what kind of HCN subunit contributed to the production of the AHP, they provided no AHP piling-up; hence, there will be no conduction failure and no further effect of ZD7288 would be observed. In other words, whether the AHP is influenced is the key factor to influence conduction failure. Higher stimulation frequency would evoke conduction failure in A_β fibers attributed to sodium channel mechanism,[38,40] which is different from the present situation. Future validation of the key HCN isoforms underlying conduction failure would further support a causal link between HCN channels and conduction failure.

The selective action of ZD7288 on the AHP of small-diameter DRG neurons and thus C-fiber conduction failure has the potential to provide an experimental foundation for the development of a new type of peripheral analgesic therapy that (1) selectively suppresses nociceptive afferent inputs, (2) produced minimal side effects, and (3) is safe and convenient for patient use. Injection of ZD7288 perineuronally is such an operation. In this study, using HCN blockers does not affect the first phase of formalin pain but the second phase, which is supported by Young's investigation.[40] Though, this study further demonstrated that perineuronal injection of ZD7288 significantly inhibited both

mechanical and heat hyperalgesia without influencing heart and motor function. This kind of analgesic therapy may be suitable for the treatment of abnormal peripheral pain states, especially those affecting the limbs. Future work should more seriously evaluate the potential therapeutic utility of targeting intrinsic conduction failure as an analgesic mechanism.

Conflict of interest statement

The authors have no conflicts of interest to declare.

X. Wang, S. Wang, W. Wang, and J. Duan contribute equally to this work.

This work was supported by funding from the National Natural Science Foundation of China (81371241, 31300918 and 81470060).

Acknowledgements

The authors thank A. W. Roe, M. Ringkamp, R. A. Richard, and G. D. Nicol for helpful comments on the manuscript, G. P. Feng for providing Thy1-GCaMP3 transgenic mice. The authors are grateful to professor Sanjue Hu, who is co-corresponding author.

Appendix A. Supplemental Digital Content

Supplemental Digital Content associated with this article can be found online at http://links.lww.com/PAIN/A283.

Article history:
Received 9 November 2015
Received in revised form 3 May 2016
Accepted 24 May 2016
Available online 1 June 2016

References

[1] Akerboom J, Chen TW, Wardill TJ, Tian L, Marvin JS, Mutlu S, Calderon NC, Esposti F, Borghuis BG, Sun XR, Gordus A, Orger MB, Portugues R, Engert F, Macklin JJ, Filosa A, Aggarwal A, Kerr RA, Takagi R, Kracun S, Shigetomi E, Khakh BS, Baier H, Lagnado L, Wang SS, Bargmann CI, Kimmel BE, Jayaraman V, Svoboda K, Kim DS, Schreiter ER, Looger LL. Optimization of a GCaMP calcium indicator for neural activity imaging. J Neurosci 2012;32:13819–40.

[2] Biel M, Wahl-Schott C, Michalakis S, Zong X. Hyperpolarization-activated cation channels: from genes to function. Physiol Rev 2009;89:847–85.

[3] Binshtok AM, Bean BP, Woolf CJ. Inhibition of nociceptors by TRPV1-mediated entry of impermeant sodium channel blockers. Nature 2007; 449:607–10.

[4] Chaplan SR, Guo HQ, Lee DH, Luo L, Liu C, Kuei C, Velumian AA, Butler MP, Brown SM, Dubin AE. Neuronal hyperpolarization-activated pacemaker channels drive neuropathic pain. J Neurosci 2003;23: 1169–78.

[5] Chen Q, Cichon J, Wang W, Qiu L, Lee SJ, Campbell NR, Destefino N, Goard MJ, Fu Z, Yasuda R, Looger LL, Arenkiel BR, Gan WB, Feng G. Imaging neural activity using Thy1-GCaMP transgenic mice. Neuron 2012;76:297–308.

[6] Chen TW, Wardill TJ, Sun Y, Pulver SR, Renninger SL, Baohan A, Schreiter ER, Kerr RA, Orger MB, Jayaraman V, Looger LL, Svoboda K, Kim DS. Ultrasensitive fluorescent proteins for imaging neuronal activity. Nature 2013;499:295–300.

[7] Dalle C, Eisenach JC. Peripheral block of the hyperpolarization-activated cation current (Ih) reduces mechanical allodynia in animal models of postoperative and neuropathic pain. Reg Anesth Pain Med 2005;30: 243–8.

[8] De Col R, Messlinger K, Carr RW. Conduction velocity is regulated by sodium channel inactivation in unmyelinated axons innervating the rat cranial meninges. J Physiol 2008;586:1089–103.

[9] Debanne D. Information processing in the axon. Nat Rev Neurosci 2004; 5:304–16.

[10] Debanne D, Campanac E, Bialowas A, Carlier E, Alcaraz G. Axon physiology. Physiol Rev 2011;91:555–602.

[11] Dell'Antonio G, Quattrini A, Cin ED, Fulgenzi A, Ferrero ME. Relief of inflammatory pain in rats by local use of the selective P2X7 ATP receptor inhibitor, oxidized ATP. Arthritis Rheum 2002;46:3378–85.

[12] Djouhri L, Bleazard L, Lawson SN. Association of somatic action potential shape with sensory receptive properties in guinea-pig dorsal root ganglion neurones. J Physiol 1998;513:857–72.

[13] Emery EC, Young GT, Berrocoso EM, Chen LB, McNaughton PA. HCN2 ion channels play a central role in inflammatory and neuropathic pain. Science 2011;333:1462–66.

[14] Emery EC, Young GT, McNaughton PA. HCN2 ion channels: an emerging role as the pacemakers of pain. Trends Pharmacol Sci 2012;33:456–63.

[15] Fang X, McMullan S, Lawson SN, Djouhri L. Electrophysiological differences between nociceptive and non-nociceptive dorsal root ganglion neurones in the rat in vivo. J Physiol 2005;565:927–43.

[16] Felix R, Sandoval A, Sánchez D, Gómora JC, De la Vega-Beltrán JL, Treviño CL, Darszon A. ZD7288 inhibits low-threshold Ca(2+) channel activity and regulates sperm function. Biochem Biophys Res Commun 2003;311:187–92.

[17] Gee MD, Lynn B, Cotsell B. Activity-dependent slowing of conduction velocity provides a method for identifying different functional classes of C-fibre in the rat saphenous nerve. Neuroscience 1996;73:667–75.

[18] Grossman Y, Parnas I, Spira ME. Differential conduction block in branches of a bifurcating axon. J Physiol 1979;295:283–305.

[19] Hara K, Saito Y, Kirihara Y, Sakura S. The interaction between gamma-aminobutyric acid agonists and diltiazem in visceral antinociception in rats. Anesth Analg 2004;98:1380–4.

[20] Hu SJ, Xing JL. An experimental model for chronic compression of dorsal root ganglion produced by intervertebral foramen stenosis in the rat. PAIN 1998;77:15–23.

[21] Hu SJ, Zhu J. Sympathetic facilitation of sustained discharges of polymodal nociceptors. PAIN 1989;38:85–90.

[22] Jiang YQ, Xing GG, Wang SL, Tu HY, Chi YN, Li J, Liu FY, Han JS, Wan Y. Axonal accumulation of hyperpolarization-activated cyclic nucleotide-gated cation channels contributes to mechanical allodynia after peripheral nerve injury in rat. PAIN 2008;137:495–506.

[23] Lee DH, Chang L, Sorkin LS, Chaplan SR. Hyperpolarization-activated, cation-nonselective, cyclic nucleotide-modulated channel blockade alleviates mechanical allodynia and suppresses ectopic discharge in spinal nerve ligated rats. J Pain 2005;6:417–24.

[24] McDougall JJ. Peripheral analgesia: hitting pain where it hurts. Biochim Biophys Acta 2011;1812:459–67.

[25] Moldovan M, Alvarez S, Romer Rosberg M, Krarup C. Axonal voltage-gated ion channels as pharmacological targets for pain. Eur J Pharmacol 2013;708:105–12.

[26] Postea O, Biel M. Exploring HCN channels as novel drug targets. Nat Rev Drug Discov 2011;10:903–14.

[27] Richards N, Dilley A. Contribution of hyperpolarization-activated channels to heat hypersensitivity and ongoing activity in the neuritis model. Neuroscience 2015;284:87–98.

[28] Schnorr S, Eberhardt M, Kistner K, Rajab H, Kasser J, Hess A, Reeh P, Ludwig A, Herrmann S. HCN2 channels account for mechanical (but not heat) hyperalgesia during long-standing inflammation. PAIN 2014;155:1079–90.

[29] Smith T, Al Otaibi M, Sathish J, Djouhri L. Increased expression of HCN2 channel protein in L4 dorsal root ganglion neurons following axotomy of L5- and inflammation of L4-spinal nerves in rats. Neuroscience 2015;295:90–102.

[30] Soleng AF, Chiu K, Raastad M. Unmyelinated axons in the rat hippocampus hyperpolarize and activate an H current when spike frequency exceeds 1 Hz. J Physiol 2003;552(pt 2):459–70.

[31] Song XJ, Hu SJ, Greenquist KW, Zhang JM, LaMotte RH. Mechanical and thermal hyperalgesia and ectopic neuronal discharge after chronic compression of dorsal root ganglia. J Neurophysiol 1999;82:3347–58.

[32] Song Y, Li HM, Xie RG, Yue ZF, Song XJ, Hu SJ, Xing JL. Evoked bursting in injured Abeta dorsal root ganglion neurons: a mechanism underlying tactile allodynia. PAIN 2012;153:657–65.

[33] Sun W, Miao B, Wang XC, Duan JH, Wang WT, Kuang F, Xie RG, Xing JL, Xu H, Song XJ, Luo C, Hu SJ. Reduced conduction failure of the main axon of polymodal nociceptive C-fibres contributes to painful diabetic neuropathy in rats. Brain 2012;135:359–75.

[34] Thalhammer JG, Vladimirova M, Bershadsky B, Strichartz GR. Neurologic evaluation of the rat during sciatic nerve block with lidocaine. Anesthesiology 1995;82:1013–25.

[35] Tsantoulas C, Zhu L, Yip P, Grist J, Michael GJ, McMahon SB. Kv2 dysfunction after peripheral axotomy enhances sensory neuron responsiveness to sustained input. Exp Neurol 2014;251:115–26.

[36] Weidner C, Schmelz M, Schmidt R, Hansson B, Handwerker HO, Torebjork HE. Functional attributes discriminating mechano-insensitive and mechano-responsive C nociceptors in human skin. J Neurosci 1999; 19:10184–90.

[37] Weng XC, Smith T, Sathish J, Djouhri L. Chronic inflammatory pain is associated with increased excitability and hyperpolarization-activated current (I-h) in C- but not A delta-nociceptors. PAIN 2012;153: 900–14.
[38] Wu Q, Henry JL. Peripheral drive in Aalpha/beta-fiber neurons is altered in a rat model of osteoarthritis: changes in following frequency and recovery from inactivation. J Pain Res 2013;6:207–21.
[39] Wu X, Liao L, Liu X, Luo F, Yang T, Li C. Is ZD7288 a selective blocker of hyperpolarization-activated cyclic nucleotide-gated channel currents? Channels (Austin) 2012;6:438–42.
[40] Young GT, Emery EC, Mooney ER, Tsantoulas C, McNaughton PA. Inflammatory and neuropathic pain are rapidly suppressed by peripheral block of hyperpolarisation-activated cyclic nucleotide-gated ion channels. PAIN 2014;155:1708–19.
[41] Zhu ZR, Liu YH, Ji WG, Duan JH, Hu SJ. Modulation of action potential trains in rabbit saphenous nerve unmyelinated fibers. Neurosignals 2013; 21:213–28.
[42] Zhu ZR, Tang XW, Wang WT, Ren W, Xing JL, Zhang JR, Duan JH, Wang YY, Jiao XY, Hu SJ. Conduction failures in rabbit saphenous nerve unmyelinated fibers. Neurosignals 2009;17:181–95.